# UNIVERSITY OF BIRMINGHAM

## Research at Birmingham

# Understanding the impact of train run-throughs on railway switches using Finite Element Analysis

Shih, Jou-Yi; Hemida, Hassan; Stewart, Edward; Roberts, Clive

Link to publication on Research at Birmingham portal

# Understanding the impact of train run-throughs on railway switches using Finite Element Analysis

J. Y. Shih, H. Hemida[*], E. Stewart, C. Roberts

Birmingham Centre for Railway Research and Education, School of Engineering, University of Birmingham, Birmingham, B15 2TT, UK

*: corresponding author; email: H.Hemida@bham.ac.uk

## Abstract

Train run-throughs on railway switches is a special issue where a train passes through non-trailable railway switches in the wrong direction. This has the potential to causes severe damage and can lead to derailment. In order to undertstand the impact of train run-throughs on railway switches, a three-dimensional (3D) Finite Element (FE) model using explicit analysis has been developed. A detailed switch model has been developed that includes all key components: stretcher bars, supplementary drive, point operating equipment. The model was validated through a specifically designed experiment where switch run-throughs were emulated on a real switch; a good agreement was found between the experimental data and the model. The model has been used to make an assessment of the locking mechanisms. The forces in each component have been assessed and investigated, and the observations of failure location and component during run-through analysis are indicated. During a run-through the supplementary drive rod and stretcher bar encounter a significant plastic deformation, and it is recommended that they should be redesigned in order to avoid plastic behaviour.

Keywords: Finite Element (FE) Analysis, locking mechanism, switch, run-through, turnout, explicit analysis

## 1. Introduction

Switch run-throughs, that is when trains pass through non-trailable railway switches in the wrong direction forcing the switch to allow the train to pass, have the potential to cause significant damage to the switch and instantaneous or a later derailment, as shown in Fig. 1. Several railway accidents have occurred around the world where switch run-throughs have been determined to be the root cause of the derailment [1].
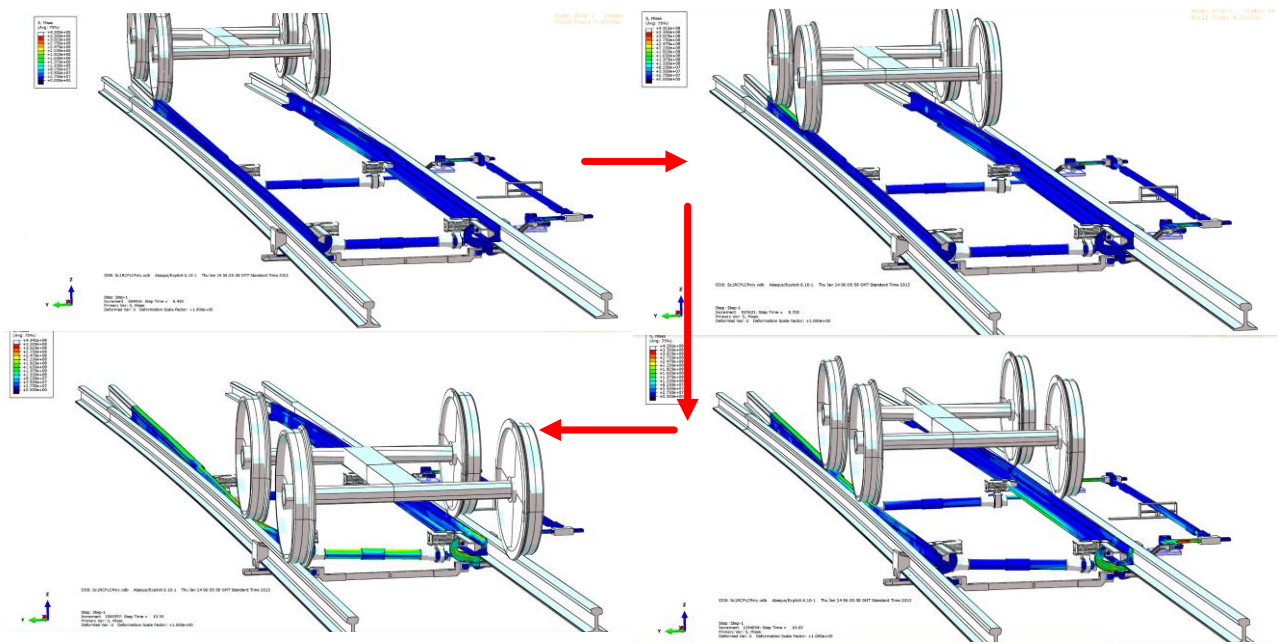
Figure 1. Demonstration of wheel-set run-through

Point Operating Equipment (POE), that is the actuator used to move a railway switch, is designed to ensure that the closed switch rail is always placed, locked and detected relative to its associated stock (fixed) rail. It is a safety requirement that the flange of a passing wheel must not come into contact with the tip of the switch and cause the wheel-set to split the switches and derail. For normal operations, POE is required to provide a minimum force, usually around 2.5 kN [2], in the facing direction to prevent the tip of the closed switch rail from opening more than 3.5 mm whilst it is locked [3].

Other safety standards may require the locking force to have a maximum limit so that, if a train happened to run through the switches whilst they are locked in the opposite direction, the locking mechanisms would give way, usually via a frangible link, to allow the wheel flange to pass between the switch and stock rail without derailing. Although a number of numerical turnout models have been developed in order to discover the optimum design in terms of track geometry, rail profile, or support stiffness [4–6], the focus is on the passage of trains in the normal direction. Furthermore, a more detailed numerical switch model is desired in order to not only investigate the effect abnormal usage and failures, which is the main reason for derailment [7,8], but also to have a full understanding of new designs.

The HW Direct Current (DC) electric point machine is considered in this paper. However, the modelling approach for a common design of Clamp Lock switch has previously been considered [9]. The aim of the present work is to develop a detailed FE model that can account for a complex switch mechanism and run-through simulation in order to allow an investigation of a better POE

2

design. The railway switch mechanism and run-through simulation are studied for a turnout to the left locked by a HW electric point mechanism with configuration variables 9.25 setup from Qdecoder (in short: cvs[10]). A numerical model is introduced first and procedures of the experimental setup are then proposed. Finally, the numerical results are validated againt the the site measurement and the locking mechanism and run-though are assessed and disscussed.

## 2. Numerical model

The main scope of the model is to investigate the forces in each component and observe the failure location and component during run-through analysis. A full FE analysis of a switch locked using a HW point machine carried out using commercial software Abaqus/Explicit is shown in Fig. 2. A structured hexahedral mesh is used in all parts and the total degree of freedom for the simulation is 1,857,174 including the contact and constraint elements. The simulation is defined in two different steps. The locking mechanism is simulated first by moving the switch blades to the lock position and in the second step, the wheel-set moves along the switch blades simulating a run-through event. The total simulation time is 15 seconds including 5 seconds for the first step and 10 seconds for the second step. The weight on the wheels (400 kN) is applied as a load (following –z direction) at the centre of the wheel-set, representing the leading wheel of a Class 66, with a train speed of 2 mph. Here a demonstration of the model development including model components, material properties, boundary conditions, constraint and contact set up is introduced. Note here the model is based on a full 3D finite element including all the deformable parts. This makes it computationally expensive and thus not recommended to be used for parametric studies.

## 2.1 Model component

A complete model of switch with the HW locking mechanism and wheel-set can be seen in Fig. 2. Here a new P8 wheel flange profile is used. The switch locking mechanisms consist essentially of switch blades, stock rails, stretcher bars, supplementary drive system, and point machine as shown in Fig. 3. Here the model is based on the Network Rail standard drawing reference in RE/PW/881 Revision C.
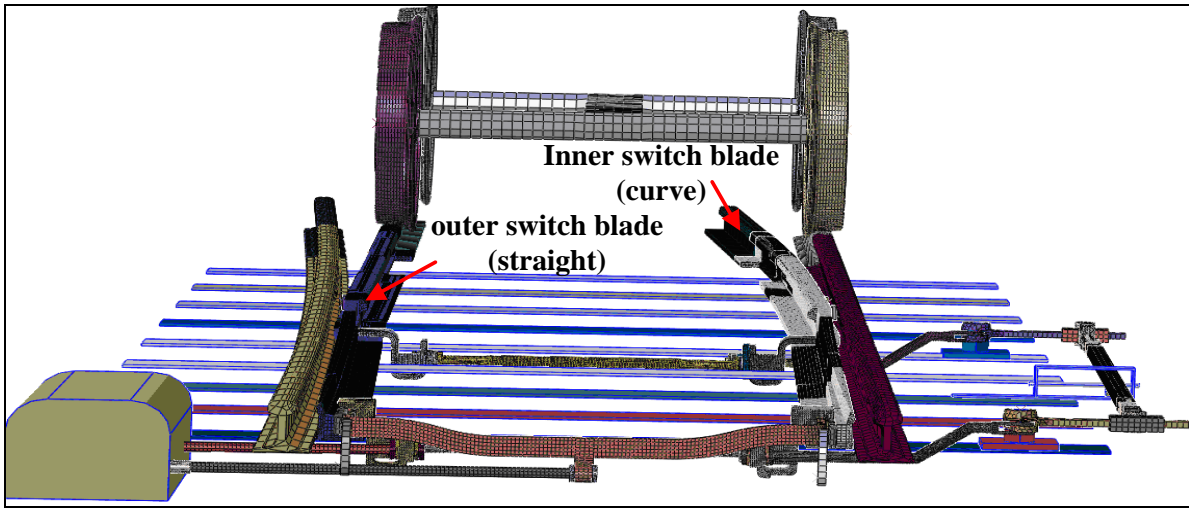
Figure 2. Complete model of switch with the HW locking mechanism and wheel-set



(a)



(b)
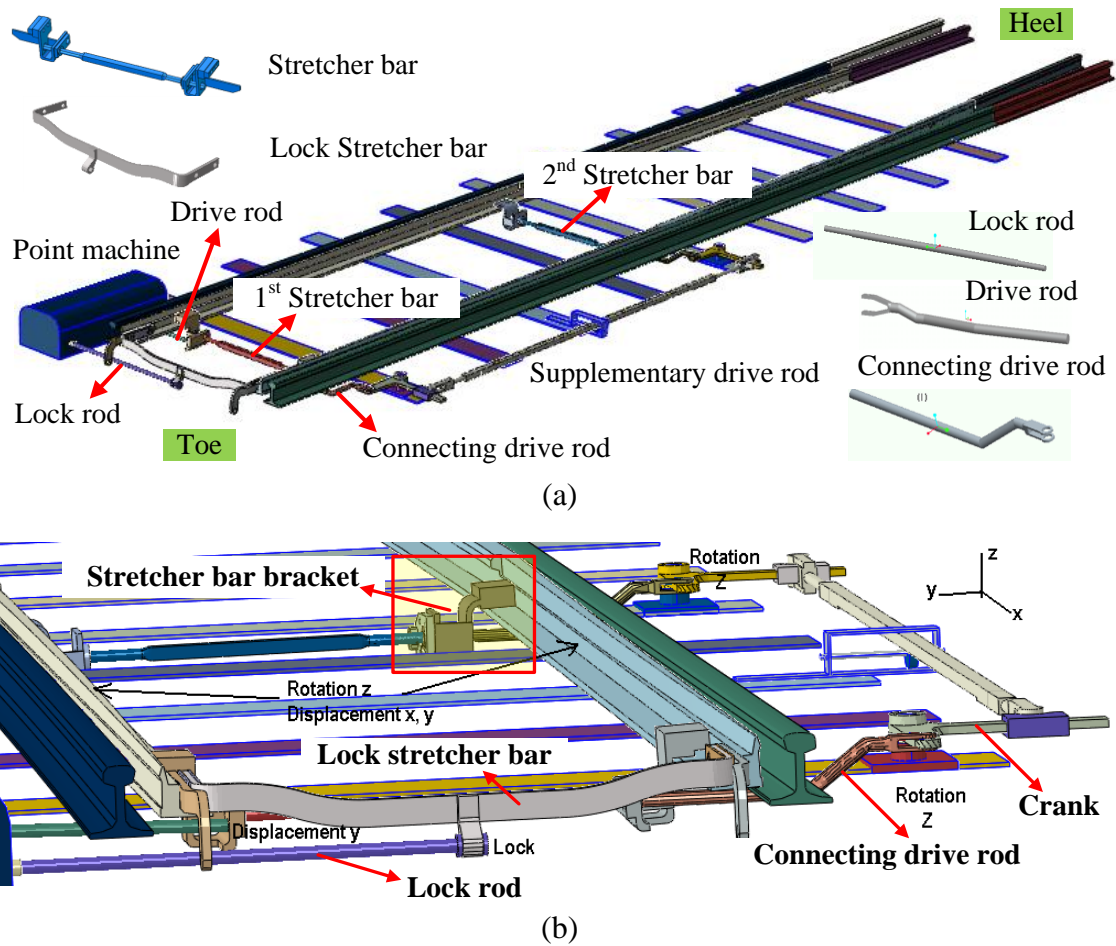
Figure 3. Complete three-dimensional model of the switch and HW electric point mechanism; (a) general view; (b) zoom in view

The 113A/UIC54B shallow depth switch and stock rail are modelled in accordance with Network Rail standard drawing references: RE/PW/807 Revision G, RE/PW/792 and RE/PW/800. Each switch blade is tapered in plan and shaped in cross-section through its length in order to prevent the wheel from climbing over the running surface [11]. Figure 3 showas sleepers, a point machine box,

4

crank base and stud, and a point rod roller assembly of the supplementary drive system. However, they are defined as display bodies for viewing purposes and thus, they are not taken in to account in the simulation.

Two drive rods are connected to the first and second stretcher bar using two cranks, which allow free rotation in the z direction (see Fig. 3(b)). The crank is then constrained by a stud with a base (see Fig. 5(b)). However, the lock stretcher bar is linked to the point machine with a movable lock rod, as shown in Fig. 3(b), and the drive rod is connected to the first stretcher bar. The two stretcher bars are connected to the switch rails with stretcher bar brackets, as shown in Fig 3. As shown in Fig. 3, the model includes a number of components with complex geometry. Therefore, a fine mesh is required in order to avoid having coarse shape elements. Furthermore, the mesh is defined to be finer in regions where interaction between parts is predominant, or in parts that have a significant role in the simulation, such as the switch blades and stretcher bar brackets. As a result, the simulation becomes very computationally expensive. In order to reduce the simulation time, some components that are less critical and do not deform easily are assumed to be rigid bodies.

## 2.2 Material properties

The lock bar, the drive, the stretcher bars, the switch blades and the cranks are modelled as deformable parts. A list of material parameters for each deformable component can be found in Table 1. Due to the fact that the switch blades are the critical component for the simulation, a detailed material specification is implemented based on data available in literature [12]. The engineering stress-strain curve is specified by the standard; however, the true stress-strain curve is required for this simulation. The true stress-strain value can be calculated by:

$$\sigma_{true} = \sigma_{eng}(1 + \varepsilon_{eng})\tag{1}$$

$$\varepsilon_{true} = \ln(1 + \varepsilon_{eng}) - \frac{\sigma_{true}}{E}\tag{2}$$

where $\varepsilon_{eng}$, $\sigma_{eng}$ is the engineering strain and stress and $E$ is the Young's modulus of the material. Here the stock rail is assumed to be rigid due to its very small deformation compared to the switch blades during run-through. This is because the second moment of inertia for the switch blade is much smaller than that for the stock rail. Furthermore, unlike the stock rail, which is fixed at every sleeper with a railpad, only limited support is supplied to the switch blade in order to allow it to be movable. As a result, significant deformation occurs in the switch blades when the wheel flange tries to push away the locked switch blade during a run-through simulation.

Table 1. Material properties for different parts in the model

| Component | Material | Yield Stress | Tensile strength |
|---|---|---|---|
| Lock rod | BS 970 070M20 (En 3A) | 300 MPa | 430 MPa |
| Drive and supplementary and connecting drive rod | BS 970:070M20 | 275 MPa | 430 MPa |
| 1st and 2nd stretcher | BS 970:070M20 | 275 MPa | 430 MPa |
| Lock stretcher bar | BS EN 10025 Grade S355JO | 355 MPa | 470 MPa |
| Crank | Rail steel | 500 MPa | - |
| Brackets | BS EN 10025 (1990) Grade 430A | 275 MPa | 430/580 MPa |
| Switch Blades | Manganese steel Mn13 [13] | 300 MPa | 1260 MPa |
| Bush | Synthetic Resin Bonded | HyperElastic Mat. | HyperElastic Mat. |

## 2.3 Boundary condition

An initial displacement of 55 mm is applied to the drive rod in the y direction (transverse to the rails) to move the switch blades until one reaches the stock rail. In this setup, the lock rod is assumed to be free to move. The boundary condition of the drive rod is then released and the lock rod is assumed to be fixed for the second step (run-through step). The cranks in the supplementary drive system are allowed to rotate around the stud of the base for both steps.

The switch blades can move freely in all directions throughout the simulation. However its vertical movement is restricted in the vertical direction at the level of sleepers. Conversely, the stock rails are fixed throughout the whole simulation. The axles of the wheels are assumed to be free in all degrees of freedom, so that they can accommodate both the movement of the wheels and the movement along the switch blades, allowing for misalignments in rail height. The wheels are specified to rotate in step 2. The speed of the wheel is simulated through the value of the rotation defined and the time duration of the step. Thus, a velocity of 2 mph is applied by defining a total time of 10 seconds with a rotation of 20 radians.

## 2.4 Constraints and contact

In order to considerably reduce the computational time, the small parts such as washers, bolts and slide chair have been omitted and replaced by surface to surface constraint, "tied", rather than bolted together, as shown in Fig. 4. A tie constraint makes the translational and rotational motion, as well as all other active degrees of freedom, equal for the surfaces in contact. The isulating jacket is tied to the lateral surfaces of the lock stretcher bar and lock detection bars. The lock detection bars are tied to the switch blade's lateral surface. In the same way, the stretcher bar brackets are tied to the switch blades through the surfaces in contact. The sleeve in the supplementary drive is tied to the surface of the crank so that its position is fixed relative to the crank.

Surface to surface contact interactions are defined between the head of the switch blade and the corresponding surface on the stock rail. Contact is also defined between the wheels and the rails with a friction coefficient of 0.3. Between the stretcher bar and the brackets there is a rubber bush which deforms to let the stretcher bar rotate slightly in order to allow the relative rotation between the bar and the switch blades. Hinge connectors are defined for the wheels, so that each wheel is rotated around its corresponding axle (defining the x-axis of the hinge along the axis of the wheel) and the bogie frame is assumed to be rigid, as shown in Fig. 5



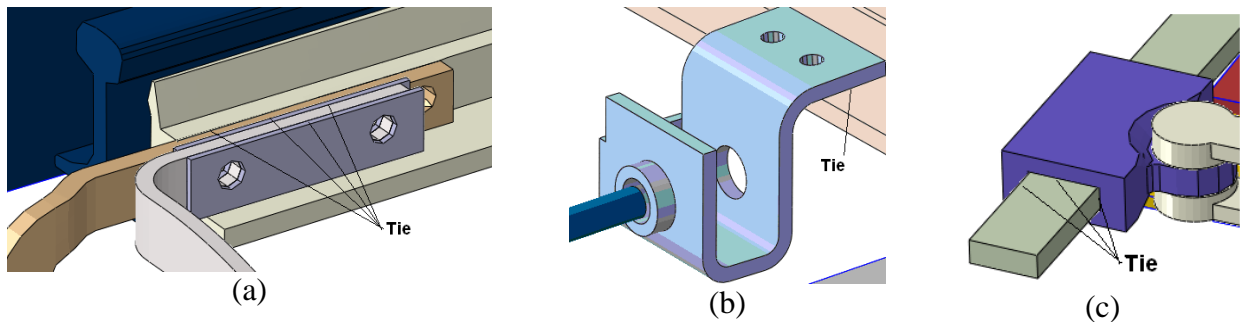<div align="center">(a)        (b)        (c)</div>

Figure 4. Tie constraints; (a) Insulating jacket, switch extension piece, lock stretcher bar and switch blade; (b) Stretcher bar bracket and switch blade foot; (c) Sleeve and crank
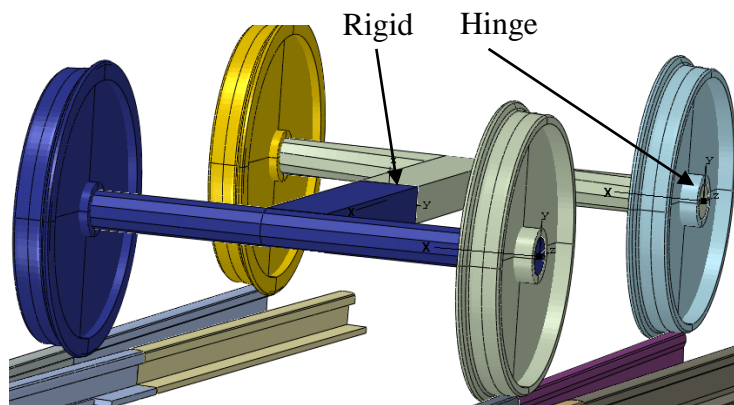


Figure 5. Hinge connectors in the model for the wheel-set

## 3. Experimental overview

In order to validate the run-through simulation model, a set of experiments were designed that emulated the run-through scenario. Hydraulic jacks were used to provide the forces that would be exterted by the wheelset during a run-through. Sensors were positioned throughout the switch inorder to collect data to validate the simulation.

## 3.1 Experimental design

In Fig. 6(a) a wheel-set is shown moving normally through a switch, while Fig. 6(b) shows the wheelset moving in the wrong direction, i.e. a run-through scenario, through the same switch. As

shown in Fig. 6(a), the distance between the gauge faces of the left-hand switch rail and the right-hand stock rail is the track gauge, nominally 1435 mm. The width of the wheel flange is around 35 mm at gauge face height, and the outside of the wheel flange stands off at around 7 mm from the gauge face. The distance between the outside edge of each of the wheel flanges is therefore $1435 - (2 \times 7) = 1421$ mm. The distance between the insides of the wheel flanges is $1435 - (2 \times 7) - (2 \times 35) = 1351$ mm.

For the run-through situation, as shown in Fig. 6(b), the wheel flanges are no longer considered to be standing off from the gauge face. Instead, they are flush against it. The wheel-set is now running hard against the gauge faces of the left-hand stock rail and the right-hand switch rail. The distance between these gauge faces is 1421 mm. The distance between the non-gauge face of the left-hand switch rail and the gauge face of the right-hand switch rail is constant regardless of the geometry of the switch rail at different distances from the toe, this could therefore be used to setup the spread of a simulated axle. This distance is equal to $1421 - 35 = 1386$ mm. As a result, the run-through simulation is set up based on the width of a wheel flange (35 mm) and the distance between the non-gauge face of the left hand switch rail to the right-hand switch rail (1386 mm), as shown in Fig. 6(b). More detail can be seen in Section 3.2.
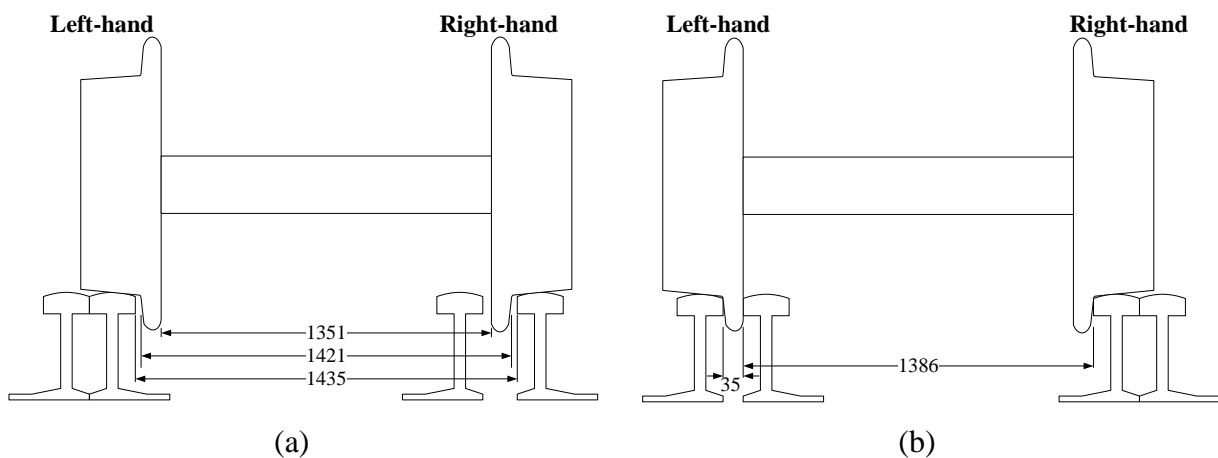


Figure 6. Passage of a wheel-set from the reverse side, with points normal; (a) typical running; (b) run-through

## 3.2 Experimental procedure

The run through was simulated by setting the points to the normal position, then emulating a wheel-set progressing along the points in the converging direction from the reverse direction. This was done using a hydraulic wedge spreader, as shown in Fig. 7, to open the gap between the stock and switch rails (to the width of a wheel flange) whilst using a hydraulic brace to maintain the correct gauge and ensure force is applied to both sides, as shown in Fig. 8.

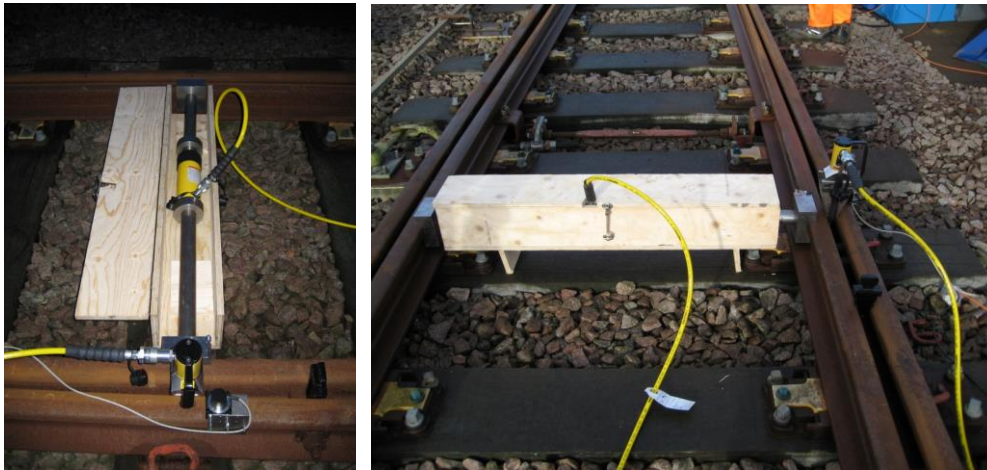Figure 7. The wedge spreader used to simulate the run-through



Figure 8. The hydraulic equipment; (a) without the safety case; (b) with the safety case in place

Wedge spreading began 6500 mm from the tip of the switch and ended at the end of the tip. However, approaching the toes of the switch, this became more difficult until finally there was insufficient room to emulate the full width of the wheel-set safely. At this point, further tests (after 3000 mm) were carried out using only the hydraulic spreader to emulate a single wheel flange between the locked side switch rail and corresponding stock rail. The steps of the experiment are as follows:

1. The wheel brace, consisting of shaped blocks, jack, and other hardware, is fitted in place and expanded to the required size.
2. The wedge spreader is fitted and expanded until the fit is tight.
3. Data acquisition commences.
4. The wedge spreader is expanded until the presence of a wheel-set is emulated at that point.
5. Data acquisition stops.

9

6. A safety wedge is inserted allowing the hydraulic wedge to be removed without closing the gap created.

7. The wheel brace is removed.

8. The process is repeated at each bearer.

A schematic of the spreader layout can be seen in Fig. 9. Pressure sensors were located in line with the wedge spreader hose and the displacement sensor was located next to the wedge spreader in order to monitor movement at the spreader to maintain consistency. A force sensor was installed on the drive rod in order to measure the force during run-through for numerical validation purposes. It can be seen that relatively good agreement was obtained between the simulation and experimental results, as shown in Fig. 10.
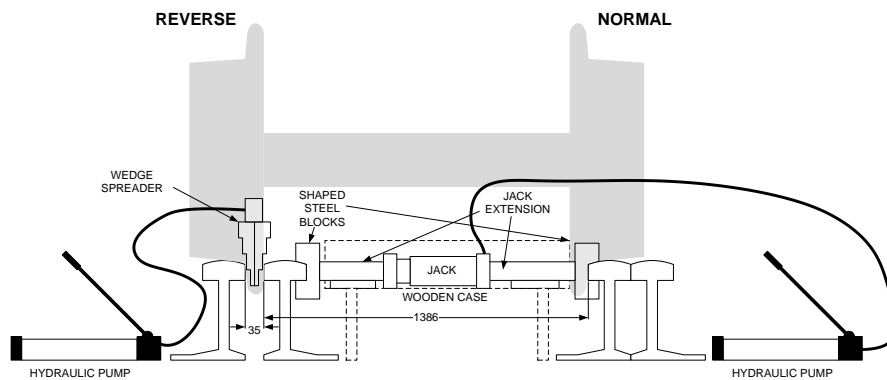


Figure 9. A representation of the wheel brace and wedge spreader in use to force the points into the reverse position



Figure 10. Comparison of the force on the drive rod from the numerical model with measurement

## 4. Numerical results

In this section, the transferred forces and the deformation of critical components during locking and run-through are analysed and disscussed. Using simulation, the failure mode and location of components affected by the run-through are identified.

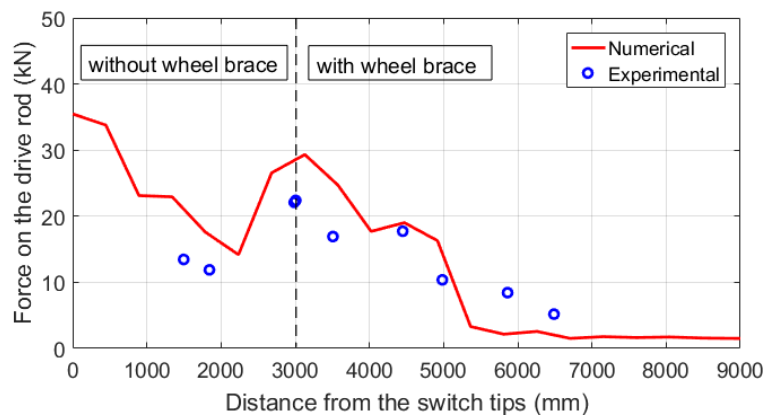The forces in the lock, drive rod and supplementary drive components during locking and run-through are shown in Fig. 11. In the case of the drive rod, the required load for closing and locking the machine is about 2 kN, which is lower than the design standard. The two peak values can be found when the wheels are approaching the stretcher bar; 18 kN as the front wheels approach the second stretcher bar and 30 kN as the back wheels pass the second stretcher bar. A sudden drop is usually found when the wheels have passed the stretcher bar. However, the force increases gradually and finally reaches the maximum drive rod force, 35 kN, at the tip of the switch blade when the wheel-set passes the first stretcher bar.

The force in the lock is much smaller than that in the drive rod during the run-through except at the position where the wheel-set is close to the first stretcher bar. The force in the lock arm is of the same order of magnitude as that of the drive rod when the wheel-set is at the first stretcher bar. The maximum force in the lock arm is approximately 31 kN at the tip of the switch.

Similar force trends to those seen in the drive rod are observed in the supplementary system. However, the forces are lower than those in the drive rod. Furthermore, the maximum force, which is around 16 kN, occurs when the front wheel is approaching the second stretcher bar, instead of at the tip of the switch.
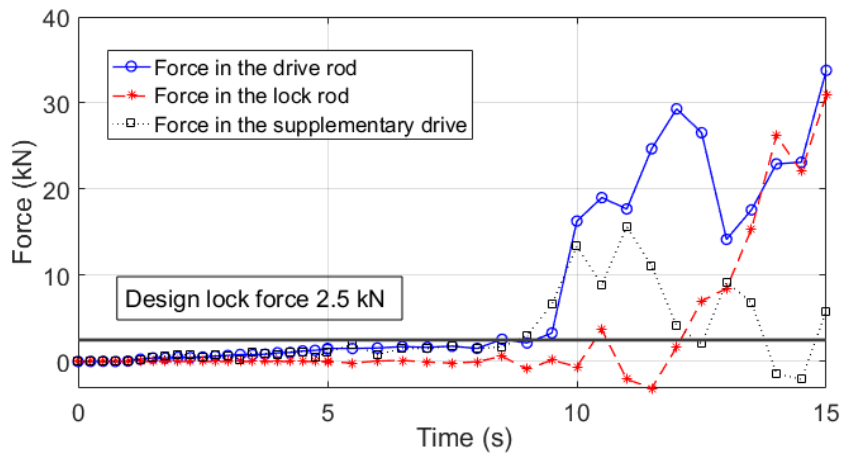


Figure 11. Force distribution duing locking and run-through simulation in three different components

Even though the force in the supplementary rod is relatively lower than in the other components, it reaches the critical buckling force during run-through, which is around 15 kN based on equation (3) [14].

$$P_{cr} = \frac{\pi^2 EI}{L^2} \tag{3}$$

The relative y displacement (transverse to the rod) of the supplementary drive rod to its original position can be seen in Fig. 12. Around 3.5 mm (~0.1% of the total length) is found after locking. The force in the supplementary rod is around 2 kN after locking (sees Fig. 11), which is much lower than the critical buckling force. However, a significant displacement of 20 mm (~0.6% of the total length) is found after run-through and eventually results in permanent deformation. The Mises stress in the supplementary drive rod is extremely high, at around 2.3 times higher than the yield stress (see Table 2).
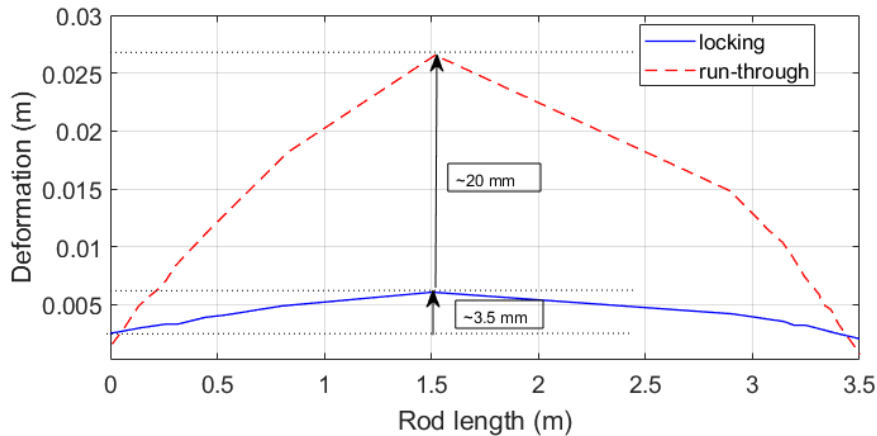


Figure 12. Supplementary drive rod deformation after locking and run-through

The maximum Mises stress and the the location of the front wheel-set position corresponding to maximum plastic deformation, and also the region where deformation remains elastic during a run-through are shown in Table 2. The maximum Mises stresses that are higher than the yield stress are indicated as bold and red. As shown, the main components which suffered significant deformation during run-through are the brackets of the stretcher bars, the switch blades, the first stretcher bar and the supplementary drive rod. These compoents reach the yield stress which results in plastic (permanent) deformation while the others remain in the elastic region. The Mises stress distribution in the worst condition for these critical components is shown in Fig. 13.

The inner switch blade (straight) undergoes significant plastic behaviour during run-through. Plastic deformations are observed at the beginning of the run-through simulation. This is because, unlike the normal situation, the rail gauge maintains 1435 mm which allows the wheel-set to run through. During run-through simulation, the rail gauge decreases while the wheel-set runs in the wrong direction (see Fig. 6). As a result, significant lateral force is applied due to the constraint of the wheel spacing. Plastic deformation for the outer switch blade (curve) occurs later, when the wheel is located 3.5 m from the tip of the switch. The outer switch rail starts to subjected to contact forces when the wheel flange starts to push away the switch blade. Therefore, no lateral force is applied

until the wheels have contact with the outer switch blade. The maximum plastic deformation is found to be 1.5 m from the toe for the inner switch and 0.7 m for the outer switch.

Table 2. Numerical results for each component

| Components | Distance from the tip (m) | | Max. Mises stress (MPa) |
| --- | --- | --- | --- |
| | Elastic region | Location of max. plastic deformation | |
| Bracket attached to inner blade at the first stretcher bar | >4.2 | 2.5 | **360** |
| Bracket attached to outer blade at the first stretcher bar | >4.2 | 2.5 | **360** |
| Bracket attached to inner blade at the second stretcher bar | >5 | 2.9 | **309** |
| Bracket attached to outer blade at the second stretcher bar | >5 | 2.9 | **296** |
| Lock stretcher bar | All | - | 344 |
| Supplementary drive rod | 0 | - | **638** |
| First stretcher bar | >4.2 | 0.7 | **280** |
| Second stretcher bar | All | - | 180 |
| Drive rod | All | - | 257 |
| Rear supplementary drive connecting rod | All | - | 142 |
| Front supplementary drive connecting rod | All | - | 254 |
| Crank | All | - | 478 |
| Inner switch blade (straight) | 0 | 1.5 | **480** |
| Outer switch blade (curve) | >3.5 | 0.7 | **490** |

Higher stresses are found for the first stretcher bar and the corresponding brackets than for the second stretcher bar. Plastic deformations are obsearved when the wheel is located 4.2 m from the toe and the maximum value is observed 2.5 m from the toe. Although no plastic behaviour is noticed in the second stretcher bar, plastic deformations are found in two connected brackets when the wheel is 5 m away from the toe. The maximum plastic deformations occur when the wheelset is 2.9 m from the toe.
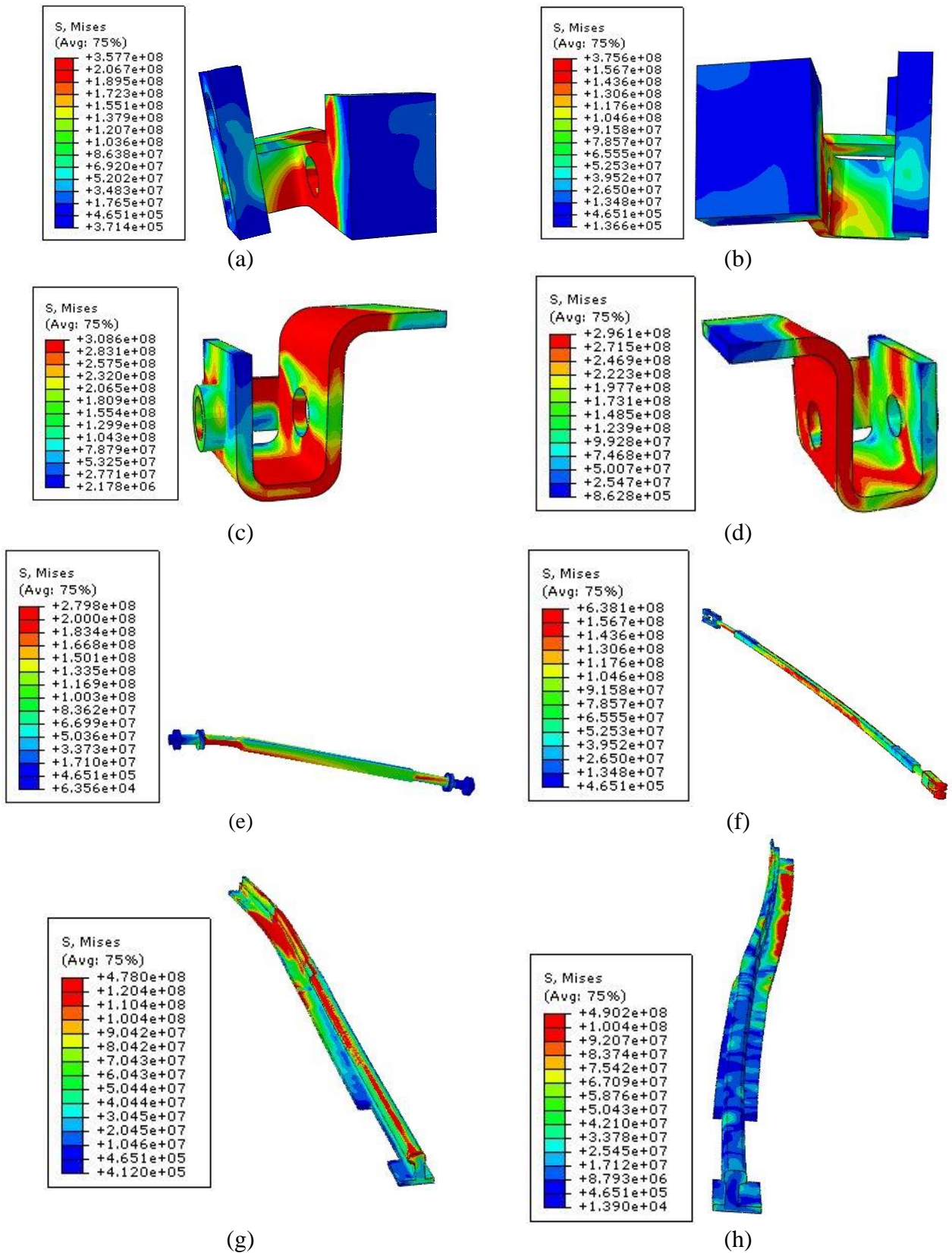
Figure 13. Mises stress distribution for each component in the worst condition; (a) the bracket attached to the inner switch blade at the first stretcher bar; (b) the bracket attached to the outer switch blade at the first stretcher bar; (c) the bracket attached to the inner switch blade at the second stretcher bar; (f) the bracket attached to the outer switch blade at the second stretcher bar; (e) the first stretcher bar; (f) supplementary drive rod; (g) inner switch blade; (h) outer switch blade

14

## 5. Conclusion

An implementation of the experiment setup for run-through analysis has been introduced and a detailed FE model has been developed using ABQUS/Explicit for a cvs 9.25 turnout locked POE using the HW point machine. Analaysis of the locking mechanism and a run-through simulation have been carried out and validated against the experiment.

Force distrubution during locking and run-through has been carried out. A force of around 2 kN force is required in order to allow the drive rod to move the switch blades to the lock position. Significant forces are observed in the drive and lock rod during run-through: 35 kN for the drive and 31 kN for the lock rod, respectively. However, no permanent displacements have been found for the drive and lock rod. They remain elastic.

On the other hand, plastic behaviour can be found for both switch rails, the first stretcher bar, all stretcher bar brackets, and the supplementary drive rod during run-through simulation. Inner switch blade and the supplementary drive rod suffer the most. The plastic deforamtions were found at the begining of the simualtion and non of the region main elastic. Buckling occurs and eventualy causes permenant deformations for the supplementary drive rod and around 20 mm of permanent lateral displacement is found after run-through.

The second stretcher bar brackets are the first parts to reach the yield stress and start to demonstrate plastic deformations 5 m from the toe. As the wheel moves further (around 0.8 m further), the bracket of the first stretcher bar starts to display plastic deformation. The second stretcher bar remains elastic throughout the whole simulation; however, the first stretcher bar demonstrates plastic behaviour. Finaly, plastic deforamtions are found in the outer curved switch blade when the wheel is 3.5 m from the toe.

An indication of wheel locations that correspond to the components starting to undergo plastic deformation during run-through have been identified. It is clear that alternative designs for the supplementary drive system and the stretcher bars are requied if the switch system is to be developed in order to prevent plastic deformation of these components during run-through events. This, in particular new stretcher bar designs, are the subject of further simulation and testing work.

authors' view and the Shift2Rail Joint Undertaking is not responsible for any use that may be made of the information it contains.

## Reference

[1] Durso FT, Gregg SE, Ferguson AN, et al. Human Factors of Run Through Switches in US Rail Operations Francis. 2014.

[2] Esveld C. Modern Railway Track. Delft University of Technology; 2001.

[3] Track System Requirements-RSSB. Railway Group Standard GC/RT5021; 2011.

[4] Pålsson BA, Nielsen JCO. Track gauge optimisation of railway switches using a genetic algorithm. Veh. Syst. Dyn. 2012;50:365–387.

[5] Nicklisch D, Kassa E, Nielsen J, et al. Geometry and stiffness optimization for switches and crossings, and simulation of material degradation. Proc. Inst. Mech. Eng. Part F-journal Rail Rapid Transit. 2010;224:279–292.

[6] Wang P, Ma X, Wang J, et al. Optimization of Rail Profiles to Improve Vehicle Running Stability in Switch Panel of High-Speed Railway Turnouts. Math. Probl. Eng. 2017;2017.

[7] Rusu MF. Automation of railway switch and crossing inspection. University of Birmingham; 2015.

[8] Hemida H, Stewart E, Roberts C. Finite Element Analysis of the Lock Stretcher Bar in a Railway Switch. Int. J. Railw. Technol. 2015;4:53–71.

[9] Hemida H, Stewart E, Roberts C. Finite Element Analysis Methodology of A Railway Switch Locked by a Rail Clamp Point Locking System. Proc. 9th Int. Conf. Eng. Comput. Technol. 2014;

[10] Qdecoder, Overview of Configuration Variables.

[11] Profillidis V. Railway management and engineering. 3rd ed. Aldershot: Ashgate; 2006.

[12] Schilke M, Ahlstrm J, Karlsson B. Low cycle fatigue and deformation behaviour of austenitic manganese steel in rolled and in as-cast conditions. Procedia Eng. [Internet]. 2010;2:623–628. Available from: http://dx.doi.org/10.1016/j.proeng.2010.03.067.

[13] Schilke M, Ahlstrm J, Karlsson B. Low cycle fatigue and deformation behaviour of austenitic manganese steel in rolled and in as-cast conditions. Procedia Eng. 2010;2:623–628.

[14] Hibbeler RC. Mechanics of Mateials. sixth edit. Person Education South Asia Pte Ltd.; 2007.